ORIGINAL PAPER

Structural characterization of human S100A16, a low-affinity calcium binder

**Elena Babini · Ivano Bertini · Valentina Borsi ·
Vito Calderone · Xiaoyu Hu · Claudio Luchinat ·
Giacomo Parigi**

Abstract The homodimeric structure of human S100A16 in the apo state has been obtained both in the solid state and in solution, resulting in good agreement between the structures with the exception of two loop regions. The homodimeric solution structure of human S100A16 was also calculated in the calcium(II)-bound form. Differently from most S100 proteins, the conformational rearrangement upon calcium binding is minor. This characteristic is likely to be related to the weak binding affinity of the protein for the calcium(II) ions. In turn, this is ascribed to the lack of the glutamate residue at the end of the S100-specific N-domain binding site, which in most S100 proteins provides two important side chain oxygen atoms as calcium(II) ligands. Furthermore, the presence of hydrophobic interactions stronger than for other S100 proteins, present in the closed form of S100A16 between the third and fourth helices, likely make the closed structure of the second EF-hand particularly stable, so even upon calcium(II) binding such a conformation is not disrupted.

Keywords S100A16 · EF-hand proteins · Calcium-binding proteins · S100 proteins · Protein dynamics

An interactive 3D complement page in Proteopedia is available at: http://proteopedia.org/wiki/index.php/Journal:JBIC:3.

Electronic supplementary material The online version of this article (doi:10.1007/s00775-010-0721-3) contains supplementary material, which is available to authorized users.

E. Babini
Department of Food Science,
University of Bologna,
Piazza Goidanich 60,
47521 Cesena, Italy

I. Bertini (✉) · V. Borsi · V. Calderone ·
X. Hu · C. Luchinat · G. Parigi
Magnetic Resonance Center (CERM),
University of Florence,
Via Luigi Sacconi 6,
50019 Sesto Fiorentino, Italy
e-mail: ivanobertini@cerm.unifi.it

I. Bertini · C. Luchinat · G. Parigi
Department of Chemistry,
University of Florence,
Via della Lastruccia 3,
50019 Sesto Fiorentino, Italy

Introduction

S100 proteins represent the largest subgroup in the family of calcium-binding proteins bearing EF-hand motifs. A functional EF-hand motif consists of a calcium(II)-binding loop (usually of about 12 amino acids) flanked by two α-helices. S100 proteins contain two EF-hand motifs, one in the N-terminal domain (composed of helix I, loop I, and helix II) and one in the C-terminal domain (composed of helix III, loop II, and helix IV). The two domains are connected by a linker, called a "hinge loop." The first N-terminal EF-hand is unconventional, because its loop is usually composed of 14 amino acids; the second one, in the C-terminal domain, is canonical. A consequence of the longer loop in the N-terminal EF-hand is the different affinity for calcium(II) with respect to the C-terminal EF-hand, due to the different ion coordination. The canonical C-terminal domain in fact binds the ion in a manner similar to calmodulin and troponin-C, resulting in a high calcium affinity [1, 2]. The N-terminal domain mostly binds the ion through main-chain carbonyl groups, in addition to the bidentate side chain of glutamate at the end of the loop, and this reduces the binding affinity up to 100 times [3].

With the exception of calbindin D_{9k}, also known as S100G, which is monomeric, all the other structures of the S100 proteins revealed a homo- and, in some cases, heterodimerization. Some members of the family also form tetramers or larger oligomers. In homodimers, the two subunits are related by a twofold axis of rotation and the major contributors to the dimer interface are helices I and IV of each subunit that are ordered in a X-type four-helix bundle. This relationship is maintained both in the apo state and in the calcium-bound state.

Upon calcium(II) binding most S100 proteins experience a conformational change that mostly involves helix III, which is antiparallel to helix IV in the apo state and rearranges itself to become almost perpendicular in the calcium(II)-bound state. This movement "opens" the structure and exposes a wide hydrophobic cleft that acts as a binding site for targets [4]. Calcium binding to the N-terminal EF-hand, instead, causes only minor alterations of its backbone conformation. On the other hand, calbindin D_{9k} does not undergo changes in its conformation upon calcium(II) binding; S100A7 does not bind calcium in the N-terminal EF-hand [5], as a consequence of the lack of the glutamate residue in the last position of loop I, the carboxylate group of which is essential for coordination of the calcium ion; and S100A10 does not bind calcium in either the N-terminal and or the C-terminal domain. Furthermore, the affinity for calcium in S100A3 is so low ($K_d = 20$ mM) that calcium binding is actually prevented in vivo.

Besides calcium(II), some S100 proteins (S100B [6], S100A2 [7], S100A7 [8], S100A12 [9]) have been shown to bind zinc(II). However, binding of zinc(II) in the cytoplasm is rather unlikely, because of its subnanomolar intracellular concentration. On the other hand, several S100 proteins have been also found in the extracellular space, where the zinc(II) concentration can be much higher [10]; in this respect, zinc was actually reported to modulate the interaction of S100B with the tau protein [11].

S100A16 is the S100 protein most widely distributed in humans, and is highly conserved in mammals [12]. Expression of most S100 proteins is actually highly tissue and cell specific, whereas S100A16 expression has been reported in a wide spectrum of human tissues (including brain), analogously to S100A2, S100A13, and S100A14. Upregulation of S100A16 was found in several cancer tissues, suggesting a function related to malignant transformation or tumor development [12]. S100A16 expression was upregulated in tumors of bladder, lung, thyroid gland, pancreas, and ovary. Furthermore, investigation of S100A16 intracellular localization in human glioblastoma cells revealed an accumulation of the protein within nucleoli and a translocation to the cytoplasm in response to calcium stimulation [13].

Among the S100 family, S100A16 is a "particular" member since it has uncommon characteristics. The N-terminal EF-hand was predicted to be functionally inactive since it comprises 15 amino acids, and lacks the conserved glutamate residue at the last position, analogously to S100A7. The inability of the N-terminal EF-hand to bind calcium was indicated by flow dialysis experiments carried out by Sturchler et al. [13]. Such experiments (performed in a high ionic strength buffer) revealed one Ca^{2+} binding site per subunit, with K_d of 430 μM, which at physiological conditions would be two- to threefold lower, thus becoming very similar to that of many other S100 proteins. Tryptophan fluorescence variations indicated the occurrence of conformational changes upon calcium(II) binding in the C-terminal EF-hand, which lead to the formation of a hydrophobic patch that could involve the hydrophobic residues in helices III and IV and in calcium-binding loop II. They also showed that S100A16 binds zinc(II) in a different site with respect to calcium(II).
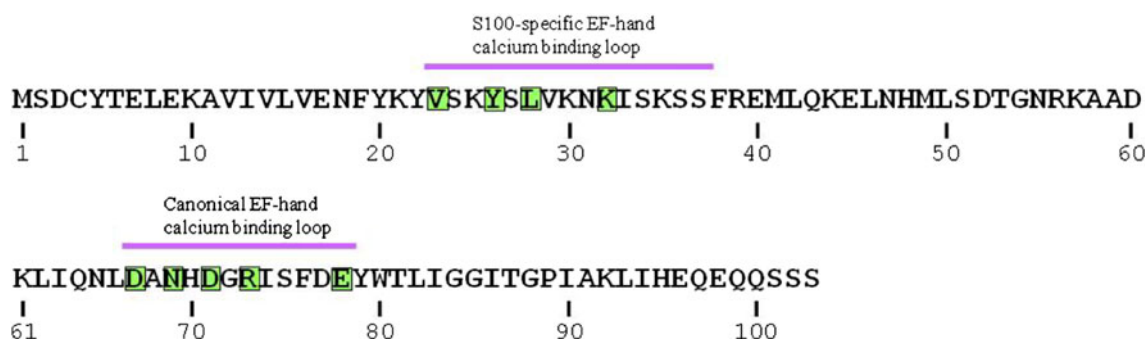
Of the 22 members found in the human genome, 17 S100 proteins have genes located in the S100A cluster on chromosome 1q21. Exceptions are S100P (located on chromosome 4p16), S100Z (5q14), S100B (21q22), and calbindin D_{9k} (Xp22) [14]. The human chromosomal region 1q21 is structurally conserved during evolution and exhibits several rearrangements which occur during tumor development. Together with the finding of upregulation of this protein in several cancer tissues [12], this indicates that S100A16 may have a role in the molecular origin of certain types of tumors and thus that it deserves structural and functional characterization studies.

Considering the uncommon behavior of S100A16 with respect to calcium binding, although several S100 protein structures are already available, the structural characterization of human S100A16 in solution has been performed in both the apo and the calcium(II) states. The apo state structure has been also solved in the crystal state. Mobility studies through relaxation rate analysis were also performed in solution. This information represents the starting point for future investigations on the binding with possible targets.

Materials and methods

Protein expression

The gene coding for human S100A16 was generated from complementary DNA using two sets of primers, in two successive runs of polymerase chain reaction (PCR), the second set intended to amplify the specific target sequence within the first, longer, run product. The first set of external primers had the following forward and reverse sequences:

S100-specific EF-hand
calcium binding loop

MSDCYTELEKAVIVLVENFYKYVSKYSLVKNKISKSSFREMLQKELNHMLSDTGNRKAAD

1   10   20   30   40   50   60

Canonical EF-hand
calcium binding loop

KLIQNLDANHDGRISFDEYWTLIGGITGPIAKLIHEQEQQSSS

61   70   80   90   100

Scheme 1 Amino acid sequence of S100A16. The residues involved in calcium(II) coordination are highlighted

OS116F1 (TGCTGGAGAGGAGGCAGA) and OS116R1 (GGAAGGTCTGGAGGGAGAAG). The second set of specific primers had the following forward and reverse sequences: OS116F2 (AAACATATGTCAGACTGCTACACG) and OS116R2 (ATAGAATTCACTAGCTGCTGCTCT). The DNA amplified by PCR was cut with restriction enzymes *Nde*I and *Eco*RI, purified from agarose gel and cloned into plasmid pET21a(+) (Novagen), prepared with the same restriction enzymes. With this expression strategy, the product of the cloned gene has the wild-type sequence of the S100A16 protein (see Scheme 1), without a tag and any additional amino acid.

Vector pET21a(+), containing the human S100A16 gene and cloned to produce the protein without a tag, was transformed in BL21-Gold *Escherichia coli* strain (Novagen). Cells were grown in Luria–Bertani medium at 37°C until an optical density of 0.7 was reached at 600 nm. The protein expression was then induced by adding 1 mM isopropyl β-D-thiogalactopyranoside. The culture was allowed to grow for 4 h and then cells were harvested by centrifugation. The cell pellet was resuspended in lysis buffer [50 mM tris(hydroxymethyl)aminomethane (Tris) pH 8.0, 200 mM KCl, 1 mM dithiothreitol (DTT), 0.5 mM Pefabloc, 10 mM EDTA], and soluble proteins were extracted by sonication followed by centrifugation. The cleared lysate was then precipitated by slowly adding streptomycin sulfate to 1% and centrifugation at 15,000g for 20 min. The supernatant was dialyzed in 50 mM Tris pH 7.0, 50 mM KCl, 1 mM DTT, 10 mM EDTA (buffer A) and loaded on a Q Sepharose FF column (Amersham) equilibrated in buffer A and eluted with a linear gradient to 50 mM Tris pH 7.0, 1 M KCl, 1 mM DTT, 10 mM EDTA. The fractions containing S100A16 were collected, added to 2 mM CaCl$_2$, and dialyzed against 50 mM Tris pH 7.4, 200 mM KCl, 1 mM DTT, 2 mM CaCl$_2$ (buffer B). The protein was then purified through hydrophobic exchange with a HiPrep phenyl FF column (Amersham) equilibrated in buffer B and eluted with 50 mM Tris pH 7.4, 200 mM KCl, 1 mM DTT, 5 mM EDTA. A final purification step was performed with size-exclusion

chromatography on a HiLoad Superdex 75 16/60 column (Amersham) equilibrated with 20 mM 2-morpholinoethanesulfonic acid (MES) pH 5.5, 200 mM KCl, 1 mM DTT, 1 mM Pefabloc. Protein expression and purity were checked at every step by sodium dodecyl sulfate polyacrylamide gel electrophoresis in 17% polyacrylamide after staining of protein bands with Coomassie blue R-250 against protein marker (Novagen).

Samples of ^{15}N- and ^{13}C,^{15}N-enriched S100A16 protein were produced as described above except for the use of M9 minimal medium containing (^{15}NH$_4$)$_2$SO$_4$ and ^{13}C-glucose as the sole nitrogen and carbon sources.

To express the selenomethionine-labeled S100A16 protein, the recombinant expression vector pET21a(+) was transformed into the methionine-auxotrophic *E. coli* B834(DE3). Cells were grown overnight in 150 mL of selenomethionine medium base supplemented with selenomethionine nutrient mix (Molecular Dimensions) and L-methionine (40 mg L^{-1}). After collection by centrifugation, cells were washed twice with water, resuspended in 1.0 mL water, and added to 1.5 L of the above-mentioned medium supplemented with L-selenomethionine (40 mg L^{-1}). Cells were grown and induced as described above. The recombinant selenomethionine-labeled S100A16 protein was purified as for the native protein except that all buffers were degassed and included a reducing reagent to avoid oxidation of selenomethionine, and a chelator to remove traces of metals that could catalyze oxidation. Full incorporation of selenomethionine was confirmed by mass spectrometry (calculated 11,764.2 Da; observed 11,762.05 Da).

Crystallization, data collection, and structure determination

Crystallization trials on apo wild-type S100A16 and its selenomethionine derivative were performed by the sitting drop method from a solution containing 0.2 M potassium citrate and 20% PEG3350 at 20°C. Hexagonal crystals started to grow overnight.

Several diffraction experiments at −173 °C were performed using synchrotron light radiation. Single-wavelength anomalous diffraction measurements were carried out on the selenium edge wavelength (0.976 Å) at beamline XRD-1 at ELETTRA (Trieste, Italy), and the high-resolution monochromatic data collection was performed at beamline BW7A at DESY-EMBL (Hamburg, Germany).

The selenomethionine derivative crystal diffracted to 2.5-Å resolution and the native crystal diffracted to 2.1-Å resolution; the crystals belonged to the hexagonal space group $P6_1$ (see below) with four molecules (i.e., two functional dimers) in the asymmetric unit and a solvent content of about 55%. The data were collected by the rotation method using 0.5° steps. The two datasets were processed using MOSFLM [15] and scaled using SCALA [16, 17] and both showed a percentage of merohedral twinning of about 10%. The statistics are shown in Table 1.

The analysis of the anomalous Patterson map performed with the program SHELXD [18, 19], using the tenfold redundant dataset collected at the selenium edge (0.976 Å), provided the positions of eight selenium atoms corresponding to two methionines per monomer. The preliminary phases obtained (figure of merit 0.25) were then improved by density modification to a figure of merit of 0.75 using a solvent content of 55% with the program autoSHARP [20, 21]. The first chain tracing after phase refinement performed by ARP/wARP [22] was able to trace 180 residues in the electron density map out of 412; the phases so obtained were then merged with the structure factors of the higher-resolution native dataset and fed into a new chain tracing procedure with BUCCANEER [23], which yielded about 350 residues. The remaining residues were then added and all the side chains were placed manually using XtalView [24]. This procedure was applied to both the possible space groups $P6_1$ and $P6_5$. The latter yielded only a small number of residues traced. Therefore, the correct space group was identified as $P6_1$.

Refinement was carried out using REFMAC5 [17, 25] on the native dataset making use of NCS and TLS restraints and taking twinning into account. Between refinement cycles, the model was subjected to manual rebuilding using XtalView [24]. Water molecules were added using the standard procedure within ARP/wARP [22]. The stereochemical quality of the refined model was assessed using the program Procheck [26]. The Ramachandran plot was of good quality with no residues in the disallowed regions.

The coordinates and structure factors were deposited in the Protein Data Bank under accession code 3NXA.

It is worth mentioning that previous attempts to solve the structure by molecular replacement were unsuccessful. This was not due to a low structural homology of the models used as templates, but to the presence of pseudosymmetry, due to the fact that the noncrystallographic axis

Table 1 Data collection and refinement statistics of the single-wavelength anomalous diffraction (*SAD*) and remote datasets

	SAD dataset	Remote dataset
Synchrotron beamline (detector)	XRD-1 at ELETTRA (MarCCD)	BW7A at DESY-EMBL (MarCCD)
λ (Å)	0.976	1.006
Spacegroup	$P6_1$	$P6_1$
Cell dimensions (Å)	$a = b = 155.96$ $c = 37.09$	$a = b = 156.57$ $c = 38.14$
Resolution (Å)	51.0–2.5 (2.64–2.50)	39.1–2.1 (2.21–2.10)
Total reflections	184,676 (17,630)	340,648 (20,115)
Unique reflections	21,191 (2,821)	29,230 (3,660)
Overall completeness (%)	96.0 (87.4)	91.6 (79.4)
Anomalous completeness (%)	87.1 (58.9)	–
R_{sym} (%)[a]	8.8 (42.3)	9.2 (39.9)
R_{pim} (%)[b]	4.4 (23.3)	2.6 (17.9)
R_{anom} (%)[c]	5.9 (22.2)	–
Multiplicity	8.7 (6.2)	11.7 (5.5)
$\langle I/\sigma(I)\rangle$	5.4 (1.8)	6.0 (1.8)
B factor from Wilson plot (Å^2)	41.3	29.5
Phases FOM before density modification	0.25	–
Phases FOM after density modification	0.75	–
Refinement statistics		
Resolution (Å)	39.1–2.1 (2.15–2.10)	
Reflections in working set	26,651 (1,666)	
Reflections in test set (9%)	2,650 (173)	
R_{cryst}/R_{free} (%)	24.7 (32.9)/29.8 (37.8)	
Protein atoms	2,994	
Water molecules	96	
RMSD bonds (Å)	0.07	
RMSD angles (deg)	4.4	
Average B factor (including metals) (Å^2)	52.50	
Residues in most favored/additional allowed/ generously allowed/disallowed regions (%)	88.7/10.1/1.2/0.0	

Numbers in *parentheses* refer to the high-resolution shell

FOM figure of merit, *RMSD* root mean square deviation

[a] $R_{sym} = \sum_h \sum_l |I_{hl}-\rangle I_h\langle |/ \sum_{\mathbf{h}} \sum_l \rangle I_h\langle$

[b] $R_{pim} = \sum_h \sum_l \left(\frac{1}{n_h-1}\right)^{\frac{1}{2}}|I_{hl} - \rangle I_h\langle |/ \sum_h \sum_l \rangle I_h\langle$

[c] $R_{anom} = \sum_{hkl} |\langle I(hkl)\rangle - \langle I(-h-k-l)\rangle|/ \sum_{hkl} (\langle I(hkl)\rangle + \langle I(-h-k-l)\rangle)$

relating the two dimers in the asymmetric unit is close to one of the crystallographic axes. An additional problem is caused by the simultaneous presence of 9–10% merohedral twinning with the operator k, h, $-l$. The latter factor also accounts for R_{cryst} and R_{free} values which are higher than might be expected from the data resolution.

Isothermal titration calorimetry

Calcium(II) binding to S100A16 was characterized by measuring the heat changes during the titration of $CaCl_2$ into the protein solution using a MicroCal (Northampton,

MA, USA) VP titration calorimeter. S100A16 and $CaCl_2$ solutions were centrifuged and degassed under vacuum conditions and equilibrated at 37 °C before titration. The sample cell contained 0.2 mM S100A16 dissolved in 20 mM MES buffer (pH 5.5) with 200 mM KCl; the reference cell contained water. The solution of 10 mM $CaCl_2$ was prepared in the same buffer used in the cell sample. Upon equilibration, titrations were performed by injecting 7-μL aliquots of 10 mM ligand ($CaCl_2$) into a 0.2 mM solution of S100A16 using the default injection rate with a 300-s interval between each injection to allow the sample to return to the baseline. The resulting titration curves were corrected using the protein-free buffer control.

NMR spectroscopy and solution structure determination

All NMR experiments for assignments were performed at 25 °C with a Bruker 500 MHz spectrometer equipped with a cryoprobe. Apo and calcium(II)-loaded S100A16 samples (0.6 and 0.8 mM, respectively) were $^{13}C,^{15}N$-labeled, in 20 mM MES, 200 mM KCl, and 1 mM DTT buffer (pH 5.5), containing 10% D_2O. Sequential assignments of the backbone resonance were achieved via HNCO, HNCA, CBCA(CO)NH and HNCACB spectra. Side chain assignments were performed through 3D (H)CCH total correlation spectroscopy, HBHA(CBCACO)HN together with ^{13}C nuclear Overhauser effect spectroscopy (NOESY) heteronuclear single quantum coherence (HSQC) and ^{15}N-NOESY HSQC experiments. Proton–proton distance restraints were derived from the analysis of 2D-NOESY, ^{15}N-NOESY-HSQC, and ^{13}C-NOESY-HSQC spectra acquired with a Bruker 900 MHz spectrometer equipped with a cryoprobe. The spectra were processed using TOPSPIN 2.0 and analyzed with CARA [27]. Backbone dihedral angles were obtained from TALOS+ [28] from the chemical shifts of N, HN, H^α, C, C^α, and C^β nuclei. The structures were calculated using the program CYANA-2.1 [29, 30] by imposing the dimer symmetry constraint (noncrystallographic symmetry constraint). The two subunits in the dimeric structure were linked together through a chain of dummy atoms with zero van der Waals radii. The calcium(II) ions were included in the calculation of the calcium-loaded form by adding new residues in the amino acid sequence. Four chains of dummy atoms with zero van der Waals radii, which can freely penetrate into the protein, each of them ending with one atom with a radius of 1.8 Å, which mimics the calcium ion, were included for this purpose. Protein ligand atoms were linked to the metal ion through upper distance limits of 3 Å, according to the structure of S100A13.

The best 30 structures out of the calculated 350 structures of the CYANA family were then subjected to restrained energy minimization with AMBER 10 [31].

Nuclear Overhauser effect (NOE) and torsion angle restraints were applied with force constants of 50 kcal mol^{-1} $Å^{-2}$ and 32 kcal mol^{-1} rad^{-2}, respectively. The programs PROCHECK-NMR [32] and WHATIF [33] were used to evaluate the quality of the structures.

Calcium(II) titration was performed with a Bruker 600 MHz spectrometer at 25 °C with 356 μM apo-S100A16 sample. ^1H–^{15}N HSQC spectra were acquired for different Ca^{2+} concentrations in solution (0.1, 0.2, 0.4, 0.8, 1.6, 3.2, 6.4, and 12.8 mM).

The coordinates of the apo and calcium(II) solution structures were deposited in the Protein Data Bank under accession codes 2L50 and 2L51, respectively.

Zinc(II) titrations were also performed on both apo-S100A16 and calcium-bound S100A16 with the same experimental conditions as for the calcium(II) titration. ^1H–^{15}N HSQC spectra were acquired for different Zn^{2+} concentrations in solution (0.1, 0.3, 0.5, 1, 2, 4, and 8 mM).

Heteronuclear relaxation measurements

^{15}N-R_1, R_2, and steady-state heteronuclear ^1H–^{15}N NOEs were measured using a 700 MHz spectrometer using standard pulse sequences [34, 35], at 25 °C. The longitudinal (R_1) and transverse (R_2) relaxation rates were determined by fitting the cross-peak intensities as a function of the delay to a single-exponential decay through the standard routines of the Sparky program [36]. The heteronuclear NOE values were obtained from the ratio of the peak height for ^1H-saturated and unsaturated spectra. The heteronuclear NOE values and their errors were estimated by calculating the mean ratio and the standard error from the available data sets. R_1, R_2, and NOE values were obtained for 91 out of the 102 assigned backbone ^NH resonances for both the apo and the calcium forms. Estimates of the reorientation time were then calculated with the model-free approach [37] and S^2 values were calculated with the program TENSOR2 [38]. Theoretical predictions of ^NH R_1 and R_2 values for apo-S100A16 and calcium(II)-loaded S100A16 were calculated using HYDRONMR [39].

Results

Isothermal titration calorimetry

Isothermal titration calorimetry (ITC) experiments were performed to investigate the binding of calcium(II) ions. The binding between apo-S100A16 and Ca^{2+} is endothermic and the reaction proceeds with a positive change in enthalpy. The ITC curve obtained, shown in Fig. 1, is hyperbolic. The best-fit analysis performed using the one binding site model yields an apparent dissociation constant
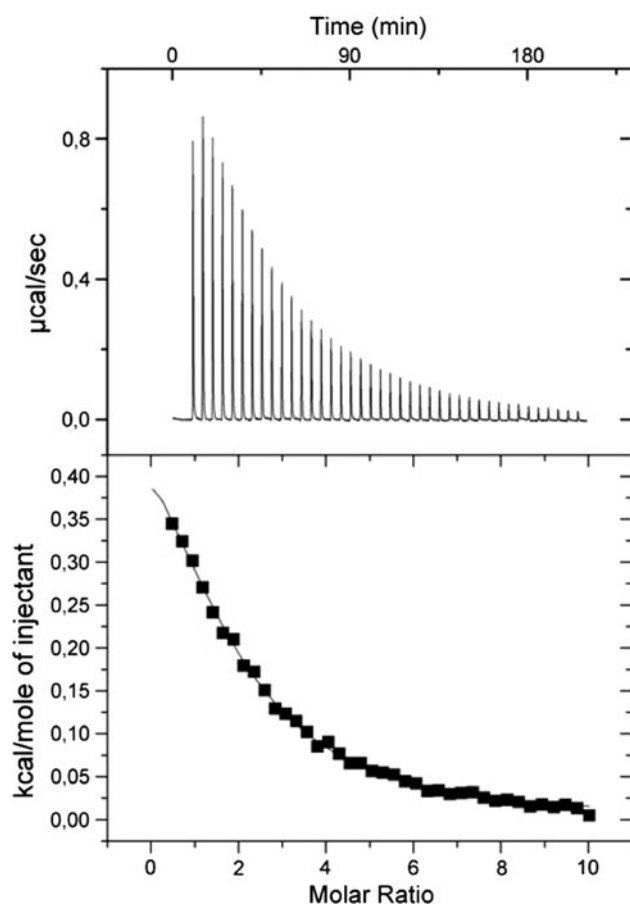
Fig. 1 Isothermograms for the binding of S100A16 to Ca^{2+}. The raw data and the fit to the one binding site model are reported in the *upper panel* and the *bottom panel*, respectively. The fit performed using a sequential two binding sites model is of similar quality. Appropriate background corrections were made to account for the heats of dilution and ionization. All experiments were performed at 25°C

of approximately $(2.7 \pm 0.2) \times 10^{-4}$ M, with 1.88 ± 0.08 binding sites per subunit. The same data were also analyzed with a sequential binding sites model, assuming the presence of two different calcium binding sites per subunit. The analysis with the two binding sites model provided relatively similar ΔH and dissociation constant values, without any significant improvement in the quality of the fit. Therefore, ITC data provide a single binding constant, as previously reported [13] and of similar value, but also suggest the possibility that calcium(II) binding could actually involve both sites in a cooperative way.

NMR resonance assignments

The ^1H–^{15}N-HSQC NMR spectra showed well-dispersed signals in both dimensions, which indicated that S100A16 is well folded in both the apo and the calcium-loaded states. All the backbone resonance signals were assigned, except those for Tyr-20 and His-95 in apo-S100A16,

Val-23 and Lys-35 in calcium(II)-loaded S100A16, and Ser-2, Lys-32, and Pro-89 in both forms.

Ca^{2+} titration of apo-S100A16

The binding of calcium(II) to apo-S100A16 was monitored by following the changes in the ^1H–^{15}N-HSQC NMR spectra of ^{15}N-labeled apo-S100A16 (Figs. S1, S2). The intensity of most peaks in or around both calcium binding regions (from Ser-24 to Ser-34 and from Asp-67 to Glu-78) decreased immediately after the addition of Ca^{2+}, becoming invisible even before reaching a 1:1 ratio between calcium(II) and S100A16. New peaks with increasing intensity then appeared with different chemical shifts when excess Ca^{2+} was added, up to a S100A16-to-calcium(II) ratio of about 1:10. This behavior is indicative of an intermediate exchange regime. In contrast, some other peaks continuously changed their chemical shifts upon increasing the Ca^{2+} concentration up to a 1:10 S100A16-to-calcium(II) ratio, as for systems in the fast exchange regime. These peaks were those experiencing a minor chemical shift perturbation. No peaks showed the typical behavior of the slow exchange regime. The analysis of the chemical shift titration thus indicates that calcium ions perturb several residues in both calcium(II)-binding loops.

Figure S3 shows the change in chemical shift during titration of some fast-exchanging residues, and the corresponding best-fit curves. A dissociation constant of about 3×10^{-4} M can be estimated assuming a cooperative binding model, as found from ITC measurements. This value is in agreement with the value obtained from ITC, and again suggests the presence of two binding sites for calcium(II). Note that both fast-exchanging residues and intermediate-exchanging residues belong to both calcium-binding loops, as the different exchange behavior during the titration depends on the difference in the chemical shift of the apo and calcium forms of the different residues.

Figure 2 shows the chemical shift perturbation on passing from the apo to the calcium(II) form of S100A16. The changes (with an average value of 0.11 ppm) are smaller than for other S100 proteins (average values of, e.g., 0.5 ppm for S100A5 and 0.37 ppm for S100A13). The residues undergoing the largest changes in chemical shifts are located in the two EF-hand loops, the calcium binding sites. The small chemical shift perturbation experienced by residues not belonging to the metal binding sites indicates that the conformational changes occurring between the apo and the calcium-bound forms are smaller than those observed for other S100 proteins.

^{15}N relaxation measurements

The relaxation parameters for apo-S100A16 and calcium-loaded S100A16 are shown in Fig. 3. The reorientation times
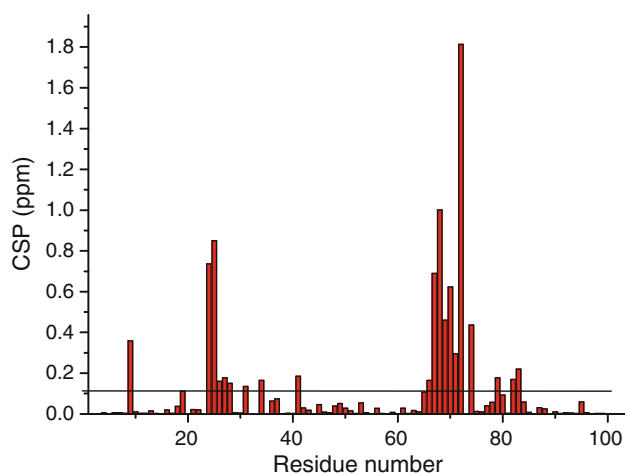
**Fig. 2** Chemical shift perturbation (*CPS*) of S100A16 upon calcium(II) binding. The *horizontal line* indicates the average value. Shift perturbations are reported as a weighted average of the amide proton and amide nitrogen shifts using the formula $\Delta\delta = [(\Delta\delta_H)^2 + (\Delta\delta_N/5)^2]^{0.5}$

corresponding to the observed relaxation rates were calculated to be 12.3 ± 1.5 and 12.3 ± 1.8 ns for the apo and calcium-loaded forms of S100A16, respectively, indicating

that the protein is dimeric in both forms, and in agreement with the molecular weight and the reorientation times observed for other S100 homodimeric proteins [40–44].

In both apo-S100A16 and calcium-loaded S100A16, the first residues in the N terminus and the residues in the C terminus are poorly structured as a result of their fast internal mobility, revealed by the small or negative NOE values, as well as by the large R_1 and the small R_2 values. Fast motion is also detected for some residues at the beginning of helix II (Ser-37, Phe-38 in the apo form; Ser-36, Phe-38 in the calcium form). Sizable motion is detected for loop L1 of the N-terminal EF-hand motif and linker L2 between the two EF-hand motifs.

Upon calcium binding, several residues are subject to an increase in mobility. Faster internal motions are present in loop L1 (the ^{1}H–^{15}N-NOE values decrease with respect to the apo form), whereas the residues at the end of helix IV (Gly-84, Ile-86, Ile-90, and Ala-91) and Asp-67 experience motions on a slower timescale, as indicated by the significantly larger R_2 value compared with the average values observed for the other residues. A reduction in mobility is, in contrast, observed upon calcium binding for the residues in loop L3 of the C-terminal EF-hand motif.
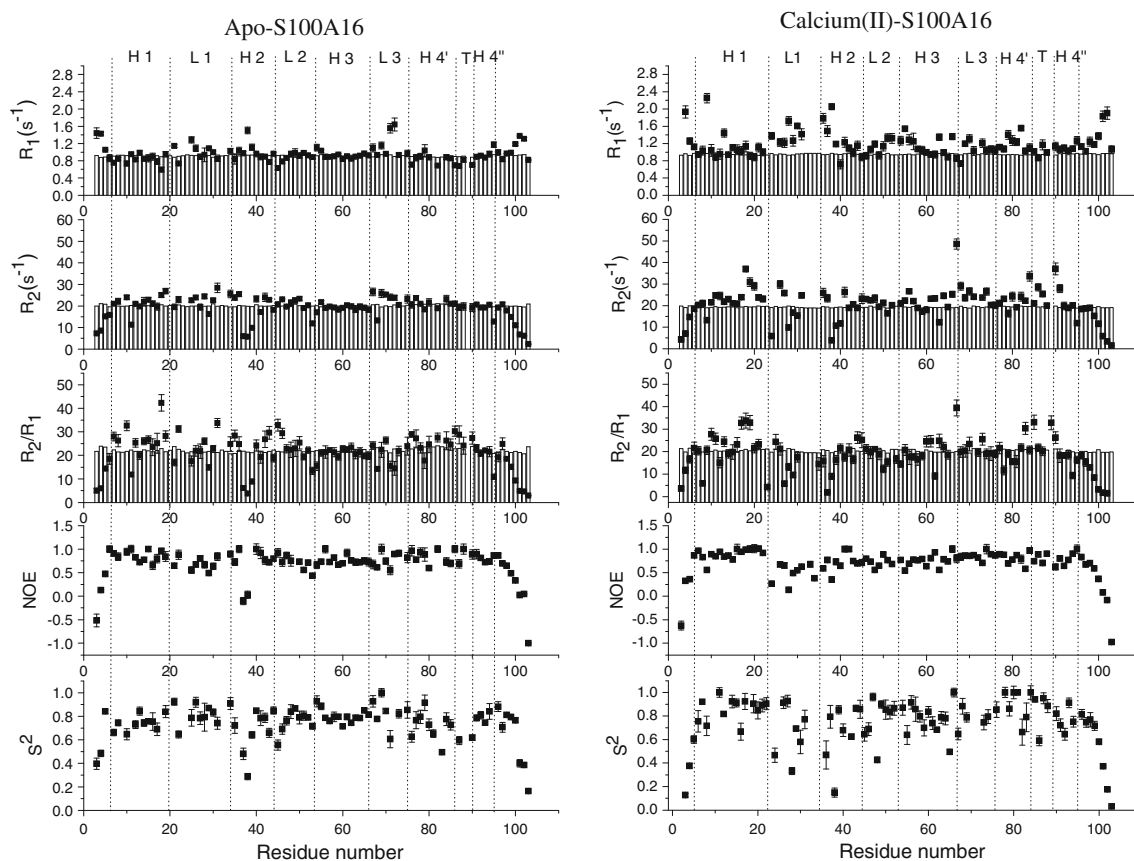
Fig. 3 Sequential plot of the experimental relaxation parameters of apo-S100A16 and calcium(II)-loaded S100A16. The values calculated with HYDRONMR are shown as *bars*

Solution structure of apo-S100A16 and calcium-loaded S100A16

The solution structures of human S100A16 in the apo and calcium-loaded forms were calculated from a total of 1,177 and 1,167 meaningful intrasubunit upper distance limits and 89 and 94 intersubunit upper distance limits for the apo and calcium forms, respectively. Few NOE patterns were detected for the residues in loop L1 between helix I and helix II and at the C terminus, consistent with the observed mobility in these regions. In the calcium form, the Ca^{2+} ions were restrained to be within 3 Å from the oxygen ligand atoms (O of Val-23, Tyr-26, Leu-28, and Lys-32 for the N-terminal Ca^{2+} binding site; OD1 of Asp-67 and Asn-69; OD1 and OD2 of Asp-71; O of Arg-73; OE1 and OE2 of Glu-78 for the C-terminal Ca^{2+} binding site).

Since no unique NOEs were detected for one subunit and not for the other, the calculations were performed by imposing the dimer symmetry constraint into the CYANA calculation. The root mean square deviation (RMSD) from the mean structure for the structured regions of the dimeric protein is 0.8 ± 0.1 Å (backbone) and 1.2 ± 0.1 Å (heavy atoms) for apo-S100A16 (residues 7–23, 35–97 of both subunits) and 0.7 ± 0.2 Å (backbone) and 1.1 ± 0.1 Å (heavy atoms) for calcium(II)-loaded S100A16 (residues 7–23, 35–97 of both subunits). PROCHECK-NMR and WHATIF programs were used to validate the structures on the Web site https://nmr.cmbi.ru.nl/icing/iCing.html. More than 98% of the residues in both apo and calcium(II) structure families were located in the allowed regions of the Ramachandran plot. The statistical analysis is reported in Table 2. The not excellent quality is common to many S100 proteins, probably owing to the property of this class of proteins (and of other signaling proteins based on the EF-hand domain) to change conformation depending on the calcium state. The relaxation rates calculated with HYDRONMR [39] from the minimized mean structures under the assumption of no internal motions, shown in Fig. 3, are in overall agreement with the averaged experimental values. This confirms that the protein is dimeric. On the other hand, the differences between the calculated and observed relaxation rates make it easier to appreciate the presence of mobility for some residues (see "[15]N relaxation measurements") [45–51].

The calculated families of structures are shown in Fig. 4. In both forms, the four helices of the two EF-hand motifs of each subunit are well defined, whereas loop L1 of the fist EF-hand motif is less well defined. These results are in line with the relaxation results. Helix IV is interrupted by residue Pro-89, after which the helical arrangement starts again.

Crystal structure of apo-S100A16

The crystal structure of apo-S100A16 was solved as described in the "Materials and methods." The statistics

Table 2 Structural restraints and statistical analysis

	Apo-S100A16	Ca(II)-S100A16
NOE upper distance limits		
Intrasubunit	1,177	1,167
Intraresidue	510	560
Interresidue		
Sequential ($|i - j| = 1$)	288	288
Medium range ($|i - j| < 4$)	236	224
Long range ($|i - j| > 5$)	143	95
Intersubunit	89	94
Dihedral angle restraints per subunit		
φ	64	62
ψ	64	62
Average RMSD from the mean (Å)		
Backbone	1.2 ± 0.2[a]	1.1 ± 0.3[a]
	0.8 ± 0.1[b]	0.7 ± 0.2[b]
Heavy	1.7 ± 0.3[a]	1.7 ± 0.4[a]
	1.2 ± 0.1[b]	1.1 ± 0.1[b]
Residual CYANA target function (Å^2)	0.7 ± 0.1	0.7 ± 0.1
Structure analysis		
Residues in most favorable regions (%)	82.1[a]	81.5[a]
	87.5[b]	87.2[b]
Residues in allowed regions (%)	13.9[a]	14.1[a]
	11.2[b]	11.4[b]
Residues in generously allowed regions (%)	2.2[a]	2.7[a]
	0.7[b]	0.9[b]
Residues in disallowed regions (%)	1.8[a]	1.7[a]
	0.6[b]	0.5[b]
Structure Z scores		
2nd-generation packing quality	−2.6 ± 0.3	−2.5 ± 0.4
Ramachandran plot appearance	−4.7 ± 0.5	−4.4 ± 0.4
χ_1/χ_2 rotamer normality	−5.7 ± 0.3	−5.3 ± 0.4
Backbone conformation	−0.8 ± 0.5	−0.7 ± 0.5
RMS Z scores		
Bond length	1.187 ± 0.002	1.184 ± 0.003
Bond angles	0.83 ± 0.01	0.86 ± 0.02
Omega angle restraints	1.9 ± 0.1	2.0 ± 0.2
Side chain planarity	2.1 ± 0.3	2.0 ± 0.2
Improper dihedral distribution	1.27 ± 0.05	1.33 ± 0.05
Inside/outside distribution	1.04 ± 0.03	1.01 ± 0.01

NOE nuclear Overhasuer effect, *RMS* root mean square

[a] Values were calculated in the sequence range 7–95 of both subunits

[b] Values were calculated in the sequence ranges 7–23 and 35–95 of both subunits

are reported in Table 1. The structure generally shows a well-defined electron density map for the four helices of the two EF-hand motifs of each subunit except for residues from 51 to 71 of monomer D, comprising helix III and part of the loop between helix III and IV. This is consistent with a very high degree of mobility of these regions in the crystal lattice, as also indicated by the B factors. To obtain reasonably low R values, the geometry weight had to be lowered in the refinement procedure, and this resulted in

Fig. 4 Solution structural families of the S100A16 subunit and ribbon representation of the homodimer mean structures of the protein in the apo and calcium(II)-bound forms. *Roman numerals* indicate the helix numbers. Calcium ligand loops are shown in *magenta*. Pro-89 is shown in *yellow*
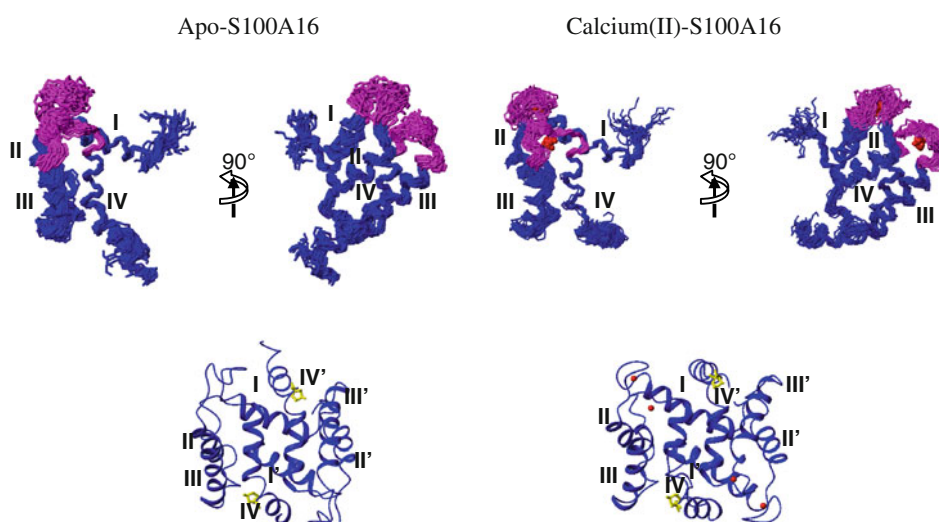
Fig. 5 a Three-dimensional structure of one of the two homodimers in the crystal structure (in *yellow*) superimposed on the mean solution NMR structure (in *blue*) of apo-S100A16, and **b** backbone root mean square deviation (*RMSD*) between the crystal structure and the mean average structure
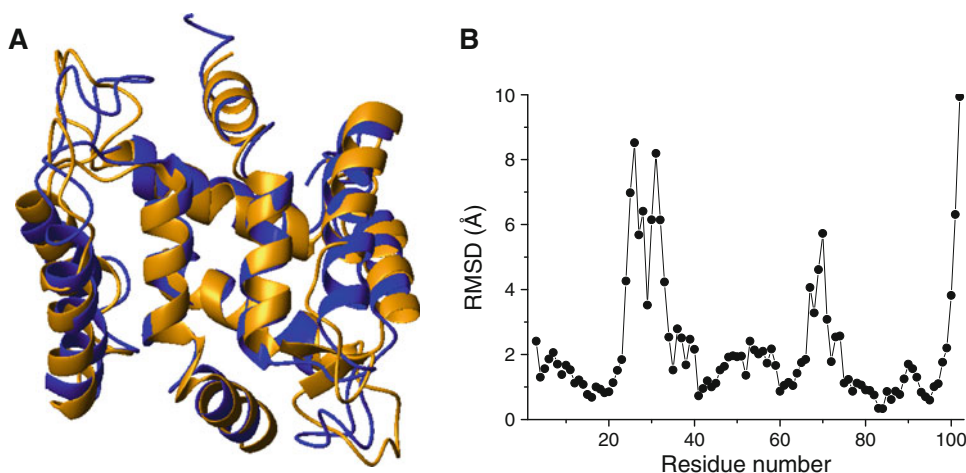
rather high RMSD for bond lengths and angles. Twinning (mainly) and pseudosymmetry (partially) are likely the reasons for this deviation from standard statistics for a crystal structure of analogous resolution.

The superposition between the mean NMR apo structure and the X-ray structure shows that the solution and solid-state structures of apo-S100A16 are in overall agreement, with the exception of loop L1 and loop L3 regions, as shown in Fig. 5. The mean backbone RMSD between the two structures of each subunit is 2.6 Å in the whole range of protein residues, but if we consider only the sequence ranges 7–23 and 35–95, it decreases to 1.7 Å, and if we exclude the two above-mentioned regions (residues 24–34 and 66–73), besides the very first and last residues at the N terminus and C terminus, which are intrinsically mobile, the RMSD decreases to 1.3 Å, indicating that the structures are in good agreement (Fig. 5). Furthermore, the disagreement is mainly due to local discrepancies rather than to overall changes in the interhelical angles (see Table 3).

Zn^{2+} and Cu^{2+} titration of apo-S100A16

After addition of Zn^{2+} to apo-S100A16, the peak intensity of the residues located in the hinge loop, in the turn region of the last helix, and at the N terminus started decreasing appreciably at a S100A16-to-zinc(II) ratio of 1:1, and some peaks disappeared when a 1:3 ratio was reached. No new peaks appeared during the whole titration, and all other peaks remained unperturbed. Similar changes were observed during the zinc(II) titration of calcium(II)-loaded S100A16.

S100A16 should thus bind zinc(II) with low affinity [dissociation constant greater than 10^{-4} M for the apo form and even larger for the calcium(II) form]. Some residues in the hinge loop (His-48) and at the N terminus (Cys-4, Glu-9) of the other subunit may constitute the Zn^{2+} ligands.

Copper(II) titration of apo-S100A16 was also attempted but the protein immediately precipitated after addition of copper(II).

Table 3 Angles between different helices, the directions of which are defined by the eight residues immediately preceding or following each EF-hand loop, calculated from the mean solution NMR structure (the errors are calculated from the standard deviations within the 30 structures of the families)

|	Apo-S100A16 (deg)	Ca(II)-S100A16 (deg)
I–II	136 ± 3 (128 ± 2)	142 ± 4
I–III	56 ± 4 (64 ± 3)	59 ± 4
I–IV	118 ± 3 (116 ± 1)	114 ± 4
II–III	157 ± 5 (163 ± 2)	144 ± 4
II–IV	52 ± 6 (37 ± 1)	60 ± 6
III–IV	148 ± 3 (153 ± 1)	150 ± 4
I–I′	136 ± 3 (154 ± 1)	138 ± 6
IV–IV′	156 ± 4 (158 ± 2)	166 ± 4

The values in *parentheses* refer to the angles calculated from the X-ray structure

Discussion

In both apo-S100A16 and calcium-loaded S100A16, dimerization mostly occurs through interactions between helices I, I′, IV, and IV′, which form an X-type helix bundle. Hydrophobic residues Trp-80 and Ile-83 in helix IV make several contacts with Leu-8, Val-12, and Leu-15 in helix I′ and with Trp-80 and Ile-83 in helix IV′ of the other subunit. Residues Glu-45, Leu-46, His-48, and Met-49 in the hinge loop between helices II and III also make contacts with residues near the N terminus of helix I′ of the other subunit. In the S100A16 dimer, all these interactions align helices I and IV in opposite directions to helices I′ and IV′, respectively.

The overall fold of the protein in the apo form is in agreement with the previously known structures for other S100 proteins [41, 44, 49, 52–54]. However, and differently from most of the other S100 proteins, it is apparent that after calcium binding S100A16 does not undergo any major conformational changes. Indeed, the backbone RMSD between the apo and the calcium(II)-loaded solution structures in the structured regions of the dimer (7–23, 35–95 of both subunits) is only 1.6 Å (Fig. 6). The C-terminal EF-hand motif does not move to the open conformation upon calcium(II) binding as shown experimentally, for instance, by the presence of strong NOEs between Ala-59 in the third helix and Ile-86 in the fourth helix.

The largest change in the solution structure of S100A16 upon calcium binding is in the angle between helices II and III, which varies from 157 ± 5° in the apo form (163 ± 2° in the crystal structure) to 144 ± 4° in the calcium-loaded form (see Table 3). The angles are measured by defining the directions of the α-helices in each EF-hand motif from the eight residues immediately preceding and following each EF-hand loop [55]. For solution structures, such values are calculated from the mean NMR structure and the
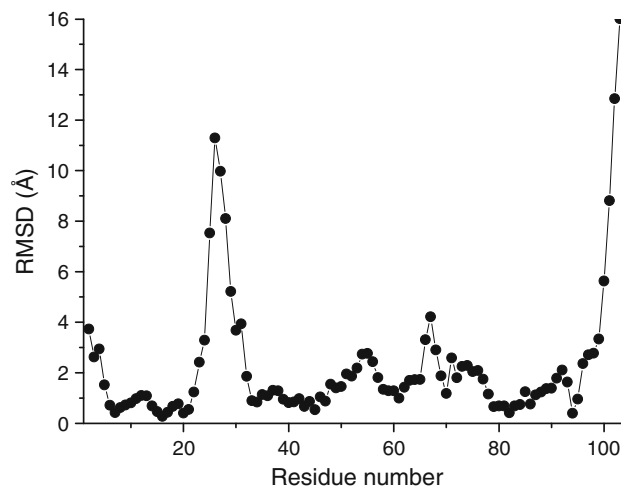
Fig. 6 Backbone RMSD between the apo-S100A16 and the calcium(II)-loaded S100A16 mean solution structures

corresponding errors from the standard deviation observed within the structures of the families. The approximately 15–20° difference in the angle between helices II and III upon calcium coordination is significantly smaller than that measured for S100A13 (40°), which is the closest neighbor of S100A16 in the phylogenetic tree.

The angle between helices III and IV is 148 ± 3° in the apoprotein (153 ± 1° if measured in the apo crystal structure), as expected for the almost antiparallel arrangement typical of EF-hand motifs in the absence of calcium. In other S100 proteins, such as S100A3, S100A5, and S100A13, such an angle typically changes by 30–50° upon calcium binding [44, 49], so the two helices become almost perpendicular [53, 56–58]. In contrast, in the calcium-loaded S100A16, the angle between helices III and IV is 150 ± 4°, so they remain almost antiparallel. Correspondingly, helices I and I′ and helices IV and IV′ make similar angles in both the apo and the calcium forms, differently from most S100 proteins.

As shown in Fig. 6, there is a significant conformational difference at the C terminus between the mean solution structures of S100A16 in the apo and calcium forms. This difference is due to the large mobility in solution of the residues after the last helix.

As already seen, the differences between the X-ray structure and the NMR structure of apo-S100A16 are mainly in the loops and in the N-terminal and C-terminal regions, due to disorder of these protein regions in solution, in this case likely due to mobility. The global orientation of the helices is, in contrast, very similar, as shown in Table 3. The global orientation of the helices is actually the main criterion to judge how much conformational change takes place.

The superposition of the NMR structure onto the crystal structure and the following symmetry expansion (coherently

with the crystallographic symmetry) does not show any significant difference in the crystal packing contacts with respect to those present in the crystal structure. This implies that the structural differences in the above-mentioned regions in the solid state are not due to packing contacts but are related to an intrinsic mobility of those regions.

A principal component analysis of the six interhelical angles representing the reciprocal orientation of the four helices [55] clearly shows the peculiar features of S100A16 within the EF-hand family. With use of the first two principal components, it is found that EF-hand proteins are clearly clustered into two subgroups (closed and open) which are characterized by the protein metal content, i.e., the apo and calcium-loaded forms. The principal component values for the two forms of S100A16 in solution were calculated from the interhelical angles reported in Table 3 and plotted together with the values previously calculated for all the other S100 proteins [49] (Fig. 7), by using the same coefficients for the interhelical angles reported in Babini et al. [55]. The principal component plot shows that apo-S100A16 is regularly positioned with respect to the other apo S100 proteins, whereas in the calcium-loaded form it is still located in the subgroup corresponding to the closed structures in the apo state. Therefore, and at
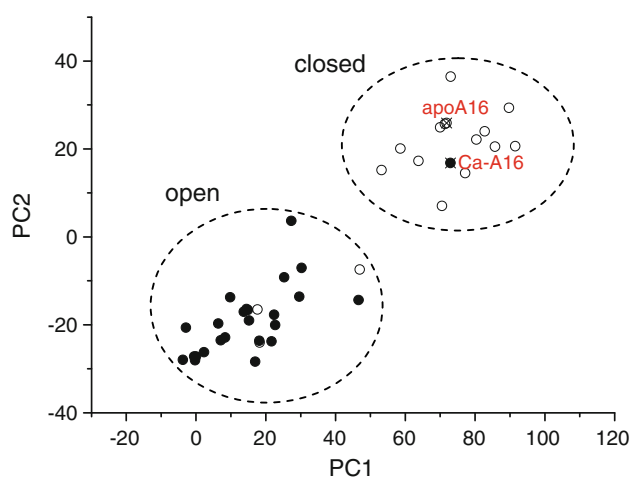

Fig. 7 Principal component plot for the S100 proteins derived from principal component analysis of the six interhelical angles. Apoproteins (S100A1, S100A2, S100A3, S100A4, S100A5, S100A6, S100A10, S100A11, S100A13, S100A16, calbindin D_{9k}) are indicated with *open circles* and calcium(II)-bound proteins (S100A1, S100A4, S100A5, S100A6, S100A7, S100A8, S100A9, S100A12, S100A13, S100A16, S100P, S100B, calbindin D_{9k}) are indicated with *solid circles*. The two *open symbols* not regularly placed with respect to the other correspond to calbindin D_{9k} and S100A10 in the apo form. The *solid symbol* not regularly placed with respect to the other corresponds to S100A16 in the calcium(II)-bound form. The data are based on the structural information reported in Table 3 and on data reported in Bertini et al. [49]. *PC1* first principal component, *PC2* second principal component

variance with all the other S100 proteins, the calcium-loaded form maintains a similar overall arrangement as the apo form. It is to be noted that the only other S100 proteins not regularly placed in the principal component plot are calbindin D_{9k} and S100A10. However, and at variance with S100A16, for both of them the apo form maintains an arrangement similar to that of the calcium-loaded form. In other words, calbindin D_{9k} and S100A10 are already in the open conformation even in the absence of calcium, whereas, in contrast, S100A16 is the first example of a calcium-loaded form which remains almost as closed as the apo form.

In most S100 proteins the two calcium binding sites are the classic EF-hand C-domain binding site and the S100-specific N-domain binding site. The former contains highly conserved calcium ligand residues at positions 1, 3, 5, 7, and 12, and has a larger affinity for the metal. The latter is a 14-residue motif where the calcium ligands are the backbone oxygen atoms of the residues at positions 1, 4, 6, and 9 and, in most cases, two side chain oxygen atoms of the residue at position 14 (usually Glu). The N-domain binding site of S100A16 lacks the glutamate at this last position (see Scheme 1). This is expected to sizably decrease the calcium binding affinity, because two important ligands are missing. Furthermore, the N-terminal EF-hand comprises 15 amino acids instead of 14, owing to the insertion, unique for S100A16, of residue Leu-28, and the ligand at position 9 is replaced by a ligand at position 10. S100A16 has been reported to bind one calcium(II) ion only for each subunit, i.e., that in the C-terminal EF-hand, through flow dialysis experiments (buffer 50 mM Tris–HCl, pH 7.5, 500 mM KCl) [13]. The present study suggests that in our conditions S100A16 indeed retains the ability to bind a calcium ion (with low affinity) also in the N-terminal EF-hand motif even without the glutamate at position 14. The calcium titration followed by NMR spectroscopy indicates that most of the residues on both calcium binding sites are in an intermediate or fast exchange regime. Chemical shifts changed until 10 equiv of calcium(II) per subunit was added, pointing out the low binding affinity for both sites.

The present observations allow us to make some general comments on the energetics involved in the calcium-triggered conformational changes that characterize the functional role of S100 proteins. To do so, reference can be made to Fig. 8a, where the calcium binding and the conformational changes are separated. As illustrated in the figure, the equilibrium constant K for the apo closed form and the calcium(II) open form is the product of the equilibrium constant for the apo and the calcium forms in the closed state (K_1) multiplied by that for the closed and open forms in the calcium(II)-bound state (K_3): $K = K_1 K_3$ ($=K_2 K_4$). For "normal" S100 proteins, $K_2 < 1$ (i.e., the apo closed form is more stable, see Fig. 8b) and $K_3 \gg 1$ (i.e.,

Fig. 8 Equilibrium constants (a) and energy levels (b–d) for the of open and closed forms of the S100 structures in the apo and calcium(II)-bound states. Observable forms of "normal" S100 proteins (b), calbindin D_{9k} (c), and S100A16 (d) are highlighted with *dashed lines*
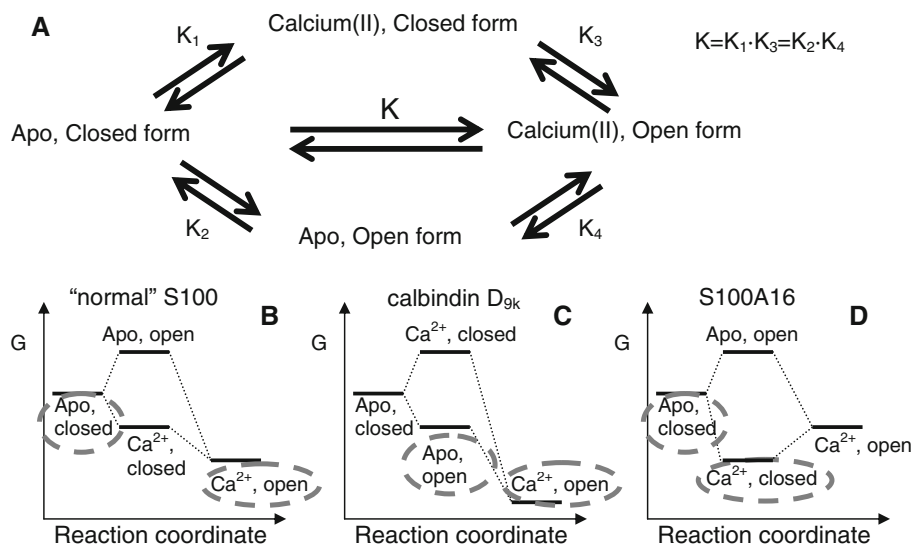

the calcium open form is more stable). In the case of calbindin D_{9k}, the apoprotein is more stable in the open form ($K_2 > 1$), i.e., in a "calcium-ready" form (Fig. 8c). Therefore, calcium binding is enhanced, as $K_4 \gg 1$. Conversely, S100A10, which also exists as apoprotein in a "calcium-ready" form, has lost its ability to bind calcium. It has been speculated that S100A10 is a structural protein that needs to always be in the open form and does not need to be opened by a signal, and therefore has lost its ability to bind calcium. Indeed, the first putative binding loop lacks three residues and cannot bind Ca^{2+} [59], and some amino acid replacements in the second putative binding loop (Asp-Cys at position 61, Glu-Ser at position 70 with respect to calbindin D_{9k}) hamper the ability of this loop to bind calcium [60]. S100A10 is in fact in a permanently activated state, having hydrophobic residues exposed even in the absence of Ca^{2+} [60, 61], which allow the protein to act as a linker tethering certain transmembrane proteins to annexin A2 and thereby assisting their traffic to the plasma membrane and/or their firm anchorage at certain membrane sites [62]. So, for both calbindin D_{9k} and S100A10, $K_2 > 1$. The case of S100A16 investigated here is an unprecedented case of $K_3 < 1$, i.e., the closed calcium-loaded form is more stable (Fig. 8d). This, of course, implies that $K_1 > 1$, despite the fact that the collective binding of the two calcium ions is relatively weak. In turn, this suggests that $K_1 > 1$ also for the "normal" S100 proteins, and that their higher calcium affinity is due to a favorable combination of both $K_1 > 1$ and $K_3 > 1$. In other words, S100A16 is somehow the opposite of calbindin D_{9k}. Whereas in normal S100 proteins calcium binding is described by the product $K = K_1 K_3$, in the case of calbindin D_{9k} and S100A16 calcium binding is only described by either K_4 or K_1, respectively. The relatively small calcium affinity of S100A16 is thus due to the low value of K_3, which makes the binding only dependent on K_1.

The presence of hydrophobic interactions represents an important factor in moving the equilibrium between the

Fig. 9 Electrostatic surface representation of the S100A16 dimer

Apo S100A16

Calcium(II)-loaded S100A16
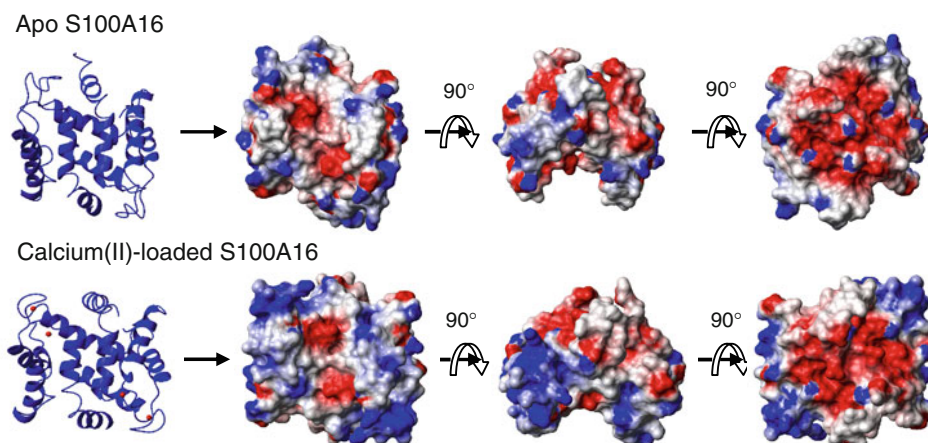
open and the closed forms in EF-hand motifs. In S100 proteins this equilibrium depends mainly on the presence/absence of interactions between the hydrophobic residues of the third and fourth helices. In S100A16 the number of hydrophobic residues present in the third helix is larger than for other S100 proteins. In the closed form of S100A16, strong interactions among hydrophobic residues are actually present between the third helix (residues Ala-58, Ala-59, Leu-62, Ile-63,and Leu-66) and the fourth helix (residues Leu-82 and Ile-86). These interactions are likely to make the closed structure of the second EF-hand particularly stable, so even upon calcium(II) binding such a conformation is not disrupted.

In S100A16, helix IV has the same length in both the apo and the calcium-bound states, differently from some other S100 proteins (S100A5, S100A6, and S100B), where it is longer in the calcium(II)-bound form than in apo form [49, 53, 63, 64]. The helix is interrupted and divided into two short helices by an 84-89 (Gly-Gly-Ile-Thr-Gly-Pro) sequence motif with three glycine residues and one proline residue. In water-soluble proteins, proline is a potent helix breaker [65]. It either breaks or kinks a helix because it cannot donate an amide hydrogen bond, and because its side chain sterically interferes with the backbone of the preceding turn. This forces a bend of about 30° in the helix axis [66, 67]. Furthermore, the glycine residues also tend to disrupt helices because their high conformational flexibility makes it entropically expensive to adopt the relatively constrained α-helical structure and because they lack hydrophobic stabilization [68].

Upon calcium binding, the global shape of the dimeric protein changes, as a result of the structural differences, as well as of the change in the distribution of surface charges. The electrostatic potential surface calculation, the results of which are shown in Fig. 9, was performed with MOLMOL [69] after inclusion of the calcium(II) charge into the AtomCharge setup file. Red and blue areas indicate negatively and positively charged regions, respectively. On passing from the apo to the calcium-loaded form, hydrophobic and positively charged residues are more exposed, whereas negatively charged residues are somewhat less exposed. These features may be important for the binding capability of the protein in the two forms. In fact, each S100 protein seems to show a peculiar surface charge and hydrophobic distribution as well as different changes upon calcium binding, ranging from exposing a more hydrophobic surface, to a larger negatively charged surface, or to a different position of charged and hydrophobic residues on the surface. This diversity is likely to be linked to the their different target specificities.

In conclusion, we have shown that the homodimeric structure of human S100A16 is subject to conformational rearrangements upon calcium(II) binding that are much smaller than those observed for most of the other S100 proteins. This is likely to be related to the weak binding affinity of the protein for the calcium(II) ions, and to the fact that the closed structure of the second EF-hand is particularly stable in the presence of strong hydrophobic interactions, so even upon calcium(II) binding such conformation is not disrupted.

References

1. Santamaria-Kisiel L, Rintala-Dempsey AC, Shaw GS (2006) Biochem J 396:201–214
2. Donato R (2003) Microsc Res Tech 60:540–551
3. Donato R (1986) Cell Calcium 7:123–145
4. Nelson MR, Chazin WJ (1998) Biometals 11:297–318
5. Brodersen DE, Etzerodt M, Madsen P, Celis JE, Thøgersen HC, Nyborg J, Kjeldgaard M (1998) Structure 6:477–489
6. Wilder PT, Baldisseri DM, Udan R, Vallely KM, Weber DJ (2003) Biochemistry 42:13410–13421
7. Randazzo A, Acklin C, Schafer BW, Heizmann CW, Chazin WJ (2001) Biochem Biophys Res Commun 288:462–467
8. Brodersen DE, Nyborg J, Kjeldgaard M (1999) Biochemistry 38:1695–1704
9. Moroz OV, Burkitt W, Wittkowski H, He W, Ianoul A, Novitskaya V, Xie J, Polyakova O, Lednev IK, Shekhtman A, Derrick PJ, Bjoerk P, Foell D, Bronstein IB (2009) BMC Biochem 10:11
10. Hwang JJ, Park MH, Choi SY, Koh JY (2005) J Biol Chem 280:11995–12001
11. Yu WH, Fraser PE (2001) J Neurosci 21:2240–2246
12. Marenholz I, Heizmann CW (2004) Biochem Biophys Res Commun 313:237–244
13. Sturchler E, Cox JA, Durussel I, Weibel M, Heizmann CW (2006) J Biol Chem 281:38905–38917
14. Ridinger K, Ilg EC, Niggli FK, Heizmann CW, Schäfer BW (1998) Biochim Biophys Acta 1448:254–263
15. Leslie AGW (1991) In: Moras D, Podjarny AD, Thierry J-C (eds) Molecular data processing. Oxford University Press, Oxford
16. Evans PR (1993) Proceedings of the CCP4 study weekend. In: Sawyer L, Isaacs N, Bailey S (eds) Data collection and processing, pp 114–122
17. Collaborative Computational Project N (1994) Acta Crystallogr D50:760–763
18. Schneider TR, Sheldrick GM (2002) Acta Crystallogr D 58:1772–1779
19. Sheldrick GM (2008) Acta Crystallogr A 64:112–122
20. Vonrhein C, Blanc E, Roversi P, Bricogne G (2007) Methods Mol Biol 364:215–230
21. Bricogne G, Vonrhein C, Flensburg C, Schiltz M, Paciorek W (2003) Acta Crystallogr D 59:2023–2030
22. Perrakis A, Morris RJH, Lamzin VS (1999) Nat Struct Biol 6:458–463
23. Cowtan K (2006) Acta Crystallogr D 62:1002–1011
24. McRee DE (1999) J Struct Biol 125:156–165
25. Murshudov GN, Vagin AA, Dodson EJ (1997) Acta Crystallogr D53:240–255
26. Laskowski RA, MacArthur MW, Moss DS, Thornton JM (1993) J Appl Crystallogr 26:283–291

27. Keller R (2004) The computer aided resonance assignment tutorial. CANTINA, Goldau
28. Shen Y, Delaglio F, Cornilescu G, Bax A (2009) J Biomol NMR 44:213–223
29. Guntert P (2004) Methods Mol Biol 278:353–378
30. Herrmann T, Güntert P, Wüthrich K (2002) J Mol Biol 319:209–227
31. Case DA, Darden TA, Cheatham TE, Simmerling CL, Wang J, Duke RE, Luo R, Merz KM, Wang B, Pearlman DA, Crowley M, Brozell S, Tsui V, Gohlke H, Mongan J, Hornak V, Cui G, Beroza P, Schafmeister CE, Caldwell JW, Ross WS, Kollman PA (2008) AMBER 10. University of California, San Francisco
32. Laskowski RA, Rullmann JAC, MacArthur MW, Kaptein R, Thornton JM (1996) J Biomol NMR 8:477–486
33. Vriend G (1990) J Mol Graphics 8:52–56
34. Kay LE, Torchia DA, Bax A (1989) Biochemistry 28:8972–8979
35. Barbato G, Ikura M, Kay LE, Pastor RW, Bax A (1992) Biochemistry 31:5269–5278
36. Goddard TD, Kneller DG (2000) SPARKY 3. University of California, San Francisco
37. Lipari G, Szabo A (1982) J Am Chem Soc 104:4546–4559
38. Dosset P, Hus JC, Marion D, Blackledge M (2001) J Biomol NMR 20:223–231
39. Garcia de la Torre JG, Huertas ML, Carrasco B (2000) J Magn Reson 147:138–146
40. Inman KG, Baldisseri DM, Miller KE, Weber DJ (2001) Biochemistry 40:3439–3448
41. Zhukov I, Ejchart A, Bierzynski A (2008) Biochemistry 47:640–650
42. Dutta K, Cox CJ, Basavappa R, Pascal SM (2008) Biochemistry 47:7637–7647
43. Bertini I, Fragai M, Luchinat C, Parigi G (2000) Magn Reson Chem 38:543–550
44. Arnesano F, Banci L, Bertini I, Fantoni A, Tenori L, Viezzoli MS (2005) Angew Chem Int Ed 44:6341–6344
45. Bertini I, Fragai M, Luchinat C, Melikian M, Mylonas E, Sarti N, Svergun D (2009) J Biol Chem 284:12821–12828
46. Bertini I, Calderone V, Fragai M, Jaiswal R, Luchinat C, Melikian M, Mylonas E, Svergun D (2008) J Am Chem Soc 130:7011–7021
47. Bertini I, Gupta YK, Luchinat C, Parigi G, Schlörb C, Schwalbe H (2005) Angew Chem Int Ed 44:2223–2225
48. Luchinat C, Parigi G (2007) J Am Chem Soc 129:1055–1064
49. Bertini I, Dasgupta S, Hu X, Karavelas T, Luchinat C, Parigi G, Yuan J (2009) J Biol Inorg Chem 14:1097–1107
50. Brüschweiler R (2003) Curr Opin Struct Biol 13:175–183
51. Bernadò P, Garcìa de la Torre J, Pons M (2002) J Biomol NMR 23:139–150
52. Smith SP, Shaw GS (1998) Structure 6:211–222
53. Otterbein L, Kordowska J, Witte-Hoffmann C, Wang CL, Dominguez R (2002) Structure 10:557–567
54. Drohat AC, Baldisseri DM, Rustandi RR, Weber DJ (1998) Biochemistry 37:2729–2740
55. Babini E, Bertini I, Capozzi F, Luchinat C, Quattrone A, Turano M (2005) J Proteome Res 4:1961–1971
56. Marenholz I, Heizmann CW, Fritz G (2004) Biochem Biophys Res Commun 322:1111–1122
57. Maler L, Sastry M, Chazin WJ (2002) J Mol Biol 317:279–290
58. Bhattacharya S, Chazin WJ (2003) Structure 11:738–739
59. Gerke V, Weber K (1985) EMBO J 4:2917–2920
60. Rety S, Sopkova J, Renouard M, Osterloh D, Gerke V, Tabaries S, Russo-Marie F, Lewit-Bentley A (1999) Nat Struct Biol 6:89–95
61. Kube E, Becker T, Weber K, Gerke V (1992) J Biol Chem 267:14175–14182
62. Rescher U, Gerke V (2008) Pflugers Arch J Physiol 455:575–582
63. Smith SP, Shaw GS (1998) Structure 6:211–222
64. Kilby PM, Van Eldik LJ, Roberts GC (1996) Structure 4:1041–1052
65. Jacob J, Duclohier H, Cafiso DS (1999) Biophys J 76:1367–1376
66. Richardson JS (1981) Adv Protein Chem 34:167–339
67. MacArthur MW, Thornton JM (1991) J Mol Biol 218:397–412
68. Blaber M, Zhang XJ, Matthews BW (1993) Science 260:1637–1640
69. Koradi R, Billeter M, Wüthrich K (1996) J Mol Graphics 14:51–55